Journal of Applied Polymer Science

Mechanical and Fracture Properties of Halloysite Nanotube Reinforced Vinyl-Ester Nanocomposites

Abdullah Alhuthali, It-Meng Low
Department of Imaging and Applied Physics, Curtin University, GPO Box U1987, Perth, WA 6845, Australia
Correspondence to: I.-M. Low (E-mail: j.low@curtin.edu.au)

ABSTRACT: The mechanical and fracture properties of vinyl-ester composites reinforced with halloysite nanotubes have been investigated. Enhancements in toughness are attributed to crack bridging, deflection, and localized plastic deformation, while strength improvements can be attributed to the large aspect ratio of fillers, favorable interfacial adhesion and dispersion, and inter-tubular interaction. Comparisons of experimental data on elastic modulus and mathematical models for predicting particulate polymer composites have verified the models of Paul and Guth. The aspect ratio of fillers and the degree of interfacial adhesion are crucial factors in the prediction of elastic modulus in these polymer nanocomposites. © 2013 Wiley Periodicals, Inc. J. Appl. Polym. Sci. 130: 1716–1725, 2013

KEYWORDS: composites; mechanical properties; nanostructured polymers; nanotubes; graphene and fullerenes

Received 19 November 2012; accepted 10 February 2013; Published online 6 May 2013
DOI: 10.1002/app.39348

INTRODUCTION

Polymer nanocomposites are blended polymer-based materials that contain one or more dimensions at the nano-scale level.[1] The presence of nano-fillers gives the material an extremely large surface area, an attribute that facilitates both rapid phase interaction and greater interfacial matrix interaction overall. It is this increased surface area that underpins the extraordinary properties of polymer nanocomposites.[2,3] The desirable aspect ratios and reduced pre-requisite for nano-fillers also lead to improved interfacial adhesion with the matrix. As such, polymer nanocomposites have superior advantages over pure and conventional composites in terms of mechanical, electrical, barrier, and thermal properties.[4–6]

Halloysite nanotubes (HNTs) are chemically similar to kaolin[7] and feature a two-layered aluminosilicate structure with hollow tubular morphology formed by rolling of layers.[8] The cylindrical shape of HNTs results from the tetrahedral and octahedral structure mismatch.[9] The lengths of the hollow tubes are between 1–15 μm with 10–30 nm inner and 50–70 nm outer diameters. This structure provides HNTs with a high aspect ratio and a very high surface area to promote a comprehensive filler and matrix interaction.[10] The hollow tubular structure of the fillers means that HNTs do not require exfoliation as in nanoclay platelets. HNTs can be easily dispersed in a polymer matrix, even at high weight fraction.[11] It is the rod-like geometry of HNTs, never intertwining, which makes dispersion of HNTs within the polymer even easier.[8]

In recent years, HNTs have become the subject of research attention as a new type of nano-filler for enhancing physical and mechanical properties of thermosets and thermoplastic polymers.[12] For example, Ye et al.[13] investigated the impact toughness of pure epoxy and epoxy/HNT nanocomposites. The addition of 2.3 wt % HNTs was found to increase the impact toughness from 0.54 kJ/m^2 for pure epoxy to 2.77 kJ/m^2 for the nanocomposite. They further concluded that when compared to montmorillonite (MMT), TiO_2, and other nano-filler modified epoxy nanocomposites, HNTs demonstrated a superior toughening effect. For example, only 35 and 60% increase in impact toughness was observed for epoxy/MMT nanocomposites[14] and epoxy/TiO_2 nanocomposites,[15] respectively. In contrast, a 400% increase in impact toughness was achieved for epoxy/HNTs nanocomposites.[13] In a similar study on epoxy/HNTs nanocomposites by Deng et al.,[16] they reported increases in both impact and fracture toughness without the loss of strength. These results further showed that both fracture toughness and impact toughness increased with an increase in filler content with an optimum loading of 5 wt % HNTs.

Vinyl-ester is a thermosetting polymer that has desirable mechanical properties which are suitable for coatings, adhesives, molding compounds, structural laminates, and electrical applications.[17] They are used in the fabrication of reinforced pipes, tanks, scrubbers, as well as hard-worked hull and deck structures in marine craft.[18] When compared to polyester resins, vinyl-esters higher design flexibility, better moisture resistance, better chemical resistance, excellent tensile, and flexural properties. In

fact, vinyl-ester resins have the best properties of epoxies and unsaturated polyesters. Thus, they are highly favored because of better control over cure rate and reaction conditions.[19–22]

Notwithstanding that HNTs have been used as fillers in matrices of epoxy, polystyrene, polypropylene, nylon-6, polyamide-6 among other[11,23–26], the addition of HNTs to vinyl ester is yet to be studied in depth. Thus, the motivation of this article was to investigate the feasibility of using HNTs to improve the mechanical and fracture properties of vinyl-ester resins. In particular, this study attempts to evaluate the influence of morphological factors of HNTs (i.e., filler dispersion, aspect ratio, and filler/matrix interaction) on the mechanical and fracture behavior of the resultant nanocomposites.

EXPERIMENTAL

Materials and Samples Preparation

Vinyl-ester resin (VER) was supplied by Fibreglass & Aesin Sales Pty, Australia, and ultrafine halloysite nanotubes (HNTs) were supplied by NZCC, New Zealand. According to the supplier, the elemental compositions (wt %) of HNTs were 50.4% SiO_2, 35.5% Al_2O_3, 0.25% Fe_2O_3, and 0.05% TiO_2. Pure samples of vinyl ester were prepared as controls by mixing the resin with 1.0 wt % methyl ethyl ketone peroxide (MEKP). The mixture was slowly and thoroughly mixed to ensure that no air bubbles formed within the matrix. The resultant mixture was poured into silicon moulds and left at room temperature under low vacuum (20 kPa) for 2 h, followed by curing at room temperature for 24 h. The nanocomposite samples were prepared by initially mixing the resin with 1, 3, or 5% of HNTs through the use of a high speed electrical-mixer (1200 rpm), followed by slow addition of MEKP as catalyst. The resultant mixtures were then poured into silicone molds, de-gassed in vacuum of 60 kPa at room temperature for 2 h, and cured under room conditions for 24 h. The samples were labeled as VER/1% HNTs, VER/3% HNTs, and VER/5% HNTs.

Microstructure Examination

The phase compositions of HNTs and HNT-reinforced vinyl-ester nanocomposites were characterized using a D8 Advance Diffractometer (Bruker-AXS) using copper radiations (λ = 1.5406 Å) and a LynxEye position sensitive detector. The XRD patterns of samples were collected by scanning from 3° to 50° (2θ) in steps of 0.02° using a scanning rate of 0.5°/min. The d-spacing of the layered particle was then calculated using Bragg's equation, ($\lambda = 2d \sin \theta$), where λ is the wavelength of X-rays, d is the interplanar distance, and θ is the Bragg angle. A transmission electron microscope (TEM; JEOL JEM2011, Japan) was used to study the morphologies of the HNTs and their dispersion within the matrix of vinyl-ester. Prior to TEM examination, samples of the HNTs were prepared by suspending the nanotubes in ethanol for 1 min, and then placed in ultra-sonic bath for 30 min. Then a droplet of suspension sprayed on a carbon thin film coated 400 mesh copper grid. An ultra microtome was used to prepare thin slices (~170 nm) of vinyl-ester/HNT samples for TEM examination.

A NEON 40ESB, scanning electron microscope (SEM; ZEISS, UK) was used to examine the microstructures of HNTs and fracture surfaces of the nanocomposites samples. All samples were coated with platinum prior to SEM examination to avoid charging.

Fracture Toughness

Rectangular single edge notch bend (SENB) samples of 10 mm × 10 mm × 60 mm dimension were used in fracture toughness testing. A sharp razor blade (with a notch-tip radius of 0.25 mm) was used to initiate a sharp crack on each sample. For all samples, the crack-to-width ratio (a/w) was limited to 0.5 and the span-to-width ratio (S/W) was maintained at 4. The tests were performed at room temperature with a LLOYD Material Testing Machine using a displacement rate of 1.0 mm/min. At least five samples of each batch were used and the mean value of fracture toughness was determined according to ASTM D5045-99 using the following equation:[27]

$$K_{\mathrm{IC}} = \frac{P_m S}{WD^{2/3}} f\left(\frac{a}{w}\right) \tag{1}$$

where K_{IC} is fracture toughness, P_m is the maximum load at fracture, S is the span of the sample, D is the specimen thickness, W is the specimen width, and a is the crack length, and $f(a/w)$ is the polynomial geometrical correction factor given as:[27]

$$f(a/w)=\frac{3(a/w)^{1/2}[1.99-(a/w)(1-a/w)(2.15-3.93a/w+2.7a^2/w^2)]}{2(1+2a/w)(1-a/w)^{2/3}} \tag{2}$$

Impact Toughness

A Zwick Charpy-impact tester with a 2.0 J pendulum hammer was used to determine the impact toughness at room temperature. At least five 40 mm span bar samples with varying notch lengths and razor-cracks were used. Values of impact toughness were determined according to the method of Plati and Williams[28] and calculated using the following equation:[27]

$$U = G_{\mathrm{IC}} BD\,\phi + U_0 \tag{3}$$

where G_{IC} is impact toughness, U is the measured energy, U_0 is the kinetic energy, D is the specimen thickness, B is the specimen breadth, and φ is the calibration factor for the geometry used.

Flexural Strength and Modulus

Rectangular bars with dimensions of (10 mm × 10 mm × 60 mm) were cut from the fully cured samples for three-point bend tests with a span of 40 mm to evaluate the flexural strength and flexural modulus according to ASTM D790-86. A LLOYD Material Testing Machine (5–50 kN) with a displacement rate of 1.0 mm/min was used to perform the test and all the tests were performed at room temperature. At least five samples of each group were used to evaluate flexural strength and flexural modulus. The values were recorded and analyzed with the aid of machine software (NEXYGENPlus) and the mean values were computed.

Impact Strength

A Zwick Charpy impact tester with a 2.0 J pendulum hammer was used to determine the impact strength at room temperature according to ASTM D 256-06. At least five bar samples of each

Table I. Mathematical Models Used to Compare with Experimental Data of This Work

Model Name	Model formula	Nomenclature
Reuss-Voigt[33,34]	$E_c^{Lower} = E_pE_m/[E_p(1-V_p) + E_mV_p]$	E_c = Elastic modulus of composite
	$E_c^{Upper} = E_pV_p + E_m(1-V_p)$	E_m = Elastic modulus of matrix
		V_p = Volume fraction of particles
Kerner[30,31]	$E_c/E_m = 1+\frac{V_p}{(1-V_p)}\frac{15(1-\nu_m)}{(8-10\nu_m)}$	V_m = Poisson ratio of matrix
Paul[30,31]	$E_c/E_m = \frac{1+(\delta-1)V_p^{2/3}}{1+(\delta-1)(V_p^{2/3}-V_p^{2/3})}$	$\delta = E_p/E_m$
Guth[32,33]	*For non-spherical particles* $E_c/E_m = (1 + 0.67\alpha V_p + 1.62\alpha^2V_p)$	α = Aspect ratio of the particles
Frankle-Acrivos[35,36]	$E_c/E_m = 1+\frac{9}{8}\left[\frac{V_p/\phi_{max})^{1/3}}{1-(V_p/V_{max})^{1/3}}\right]$	φ_{max} = *Maximum packing fraction of particles*

group with 40 mm span were used and the mean impact strength (σ_i) was calculated using the following equation:[29]

$$\sigma_i = \frac{E}{A} \quad (4)$$

where E is the impact energy to break a sample with a ligament area A.

Mathematical Modeling of Particulate-Reinforced Composites

There are a number of theoretical frameworks that have been developed to support the prediction of elastic modulus of polymer particulate reinforced composites. These sophisticated theories have been developed according to the requirements of different material or geometric parameters.[30,31] Conventionally, the elastic properties of a particulate–polymer composite's components (particle and matrix), its particle loading and its aspect ratio are used in determining the elastic modulus.[30] For example, for spherical particles, when the aspect ratio of particles equals unity, the elastic modulus of components and particle loading or particle size will be used to provide the composite modulus. The composite modulus is normally enhanced by adding particles to the matrix since the modulus of particles is usually much higher than that of the polymer matrices.[31,32] While the theories used for predicting elastic modulus of polymer particulate reinforced composites are to an extent satisfactory, the theories for predicting the strength and fracture toughness of particulate reinforced systems are less developed.[32,33] From this point, this study will limit the prediction of the mechanical properties of the composites to their elastic modulus. Table I outlines the name, formula, and nomenclature of six mathematical models for predicting elastic modulus. These mathematical models were used to compare experimental data from this study with the models to determine the applicability of the empirical relationships. The parameter values that correspond to the materials properties for mathematical model implementation are presented in Table II.

Table II. Values of Parameters Used in Mathematical Modeling

Parameters	Values	Reference
Average of aspect ratio of HNTs α	7[a]	
Elastic modulus of VER E_m (GPa)	2.9[b]	
Poisson ratio of matrix ν_m	0.35	37
Average of elastic modulus of HNTs E_p (GPa)	30	38,39
Maximum packing fraction ϕ_{max}	0.637	40
Density of VER	1.14[c]	
Density of HNTs	2.11[d]	

[a] Calculated based 50 numbers of HNT particles using SEM and TEM micrographs,

[b–d] Our experimental data.

RESULTS AND DISCUSSION

X-Ray Diffraction Analysis (XRD)

XRD patterns for pure HNTs and VER/HNT composites with 1, 3, and 5 wt % of HNTs are shown in Figure 1. A diffraction peak at 2θ of ~12.27° corresponding to the (001) plane can be seen in XRD pattern for pure HNTs. Two additional diffraction peaks at 2θ at ~20.15° and ~24.95° corresponding to (020) and (002) basal reflections are noticeable.[41,42] Trace amounts of quartz and feldspar are also evident and are represented by (*) and (+) respectively. The presence of these minerals in HNTs has also been noted by other researchers.[16,42]

For pure HNTs, a diffraction peak at a 2θ = 12.27° corresponds to a basal spacing of 0.721 nm. For VER/HNT composites, this diffraction peak has shifted towards lower 2θ values or larger basal spacing. The diffraction peaks, with corresponding basal spacing shown in parenthesis, for samples of VER/1% HNTs, VER/3% HNTs, and VER/5% HNTs were 11.87° (0.745 nm), 12.07° (0.733 nm), and 12.15° (0.728 nm), respectively (Table III). This increase in the basal spacing of HNTs in the composites sample suggests the existence of intercalation between vinyl-ester chains and the HNTs, thus confirming the formation of nanocomposites as also found in other studies.[10,41]

Microstructures of HNTs and Composites

SEM and TEM images of HNTS are shown in Figure 2. The images show that the majority of HNTs exist in a tubular shape, however, short tubular HNTs, and semi-rolled HNTs can also

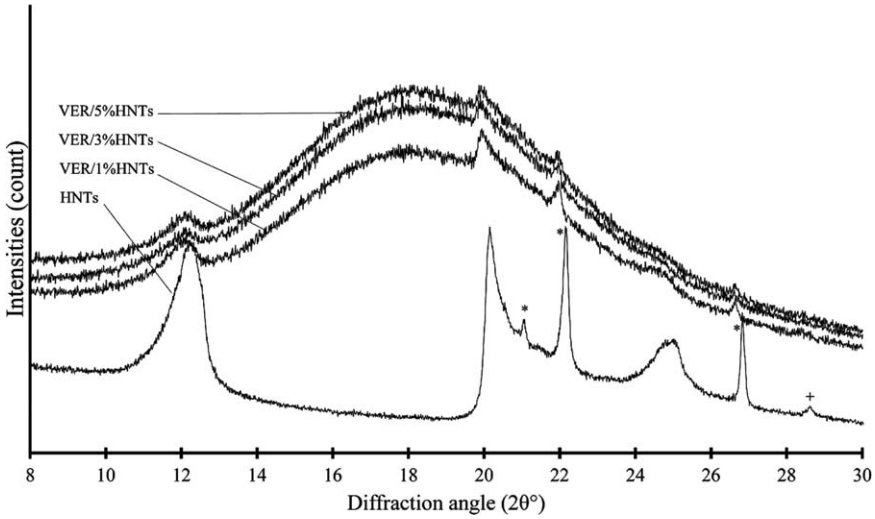

Figure 1. XRD pattern of pure HNTs and VER/HNTs composites.

Table III. XRD Results of HNTs and VER/HNTs Nanocomposites

Specific plane 2θ/d-spacing	(001)		(020)		(002)	
	2θ	d (nm)	2θ	d (nm)	2θ	d (nm)
HNTs	12.27	0.721	20.15	0.44	24.95	0.357
VER/1% HNTs	11.87	0.745	19.85	0.447	-	-
VER/3% HNTs	12.07	0.733	19.92	0.445	-	-
VER/5% HNTs	12.15	0.728	19.98	0.444	-	-

be seen. The image indicates that HNTs have a length ranging from 500 nm to 3 μm. From the image, the average outer diameters of the HNTs ranged from 100 to 300 nm whereas the average inner diameters ranged from 50 to 150 nm. The length/diameter ratio (i.e., aspect ratio) of HNTs varied between 3 and 15. Being a natural product, the size distribution of halloysite nanotubes is expected to be large.

The TEM micrographs in Figure 3(a–c) display the uniform dispersion of HNT fillers in the vinyl-ester (VER) matrix. The extent of dispersion is acceptable even though a number of micro-sized HNT clusters can be found. HNTs were randomly dispersed in the matrix with short inter-tube distances resulting in formation of HNT-rich region and long inter-tube distances resulting in VER-rich region being formed as shown in Figure 4(a). The HNT-rich regions give the appearance of HNT clusters. However, a closer examination reveals that VER has filled spaces between these clusters [Figure 4(b)]. In other words, the morphology of the HNT/VER composites displays a continuous

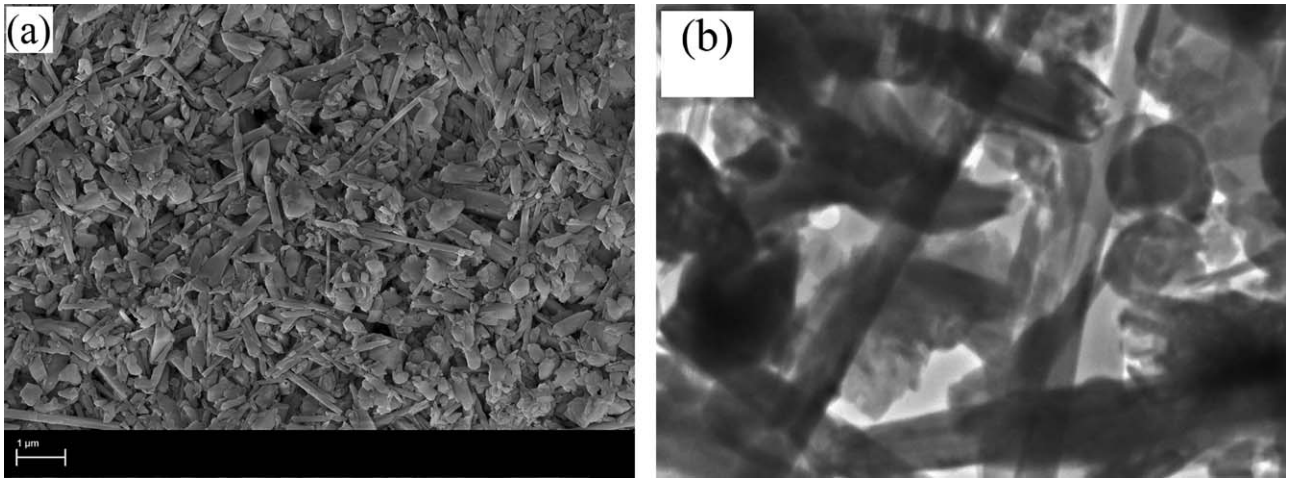

Figure 2. (a) SEM micrograph of HNTs particles and (b) TEM micrograph of HNTs particles.

Applied Polymer SCIENCE

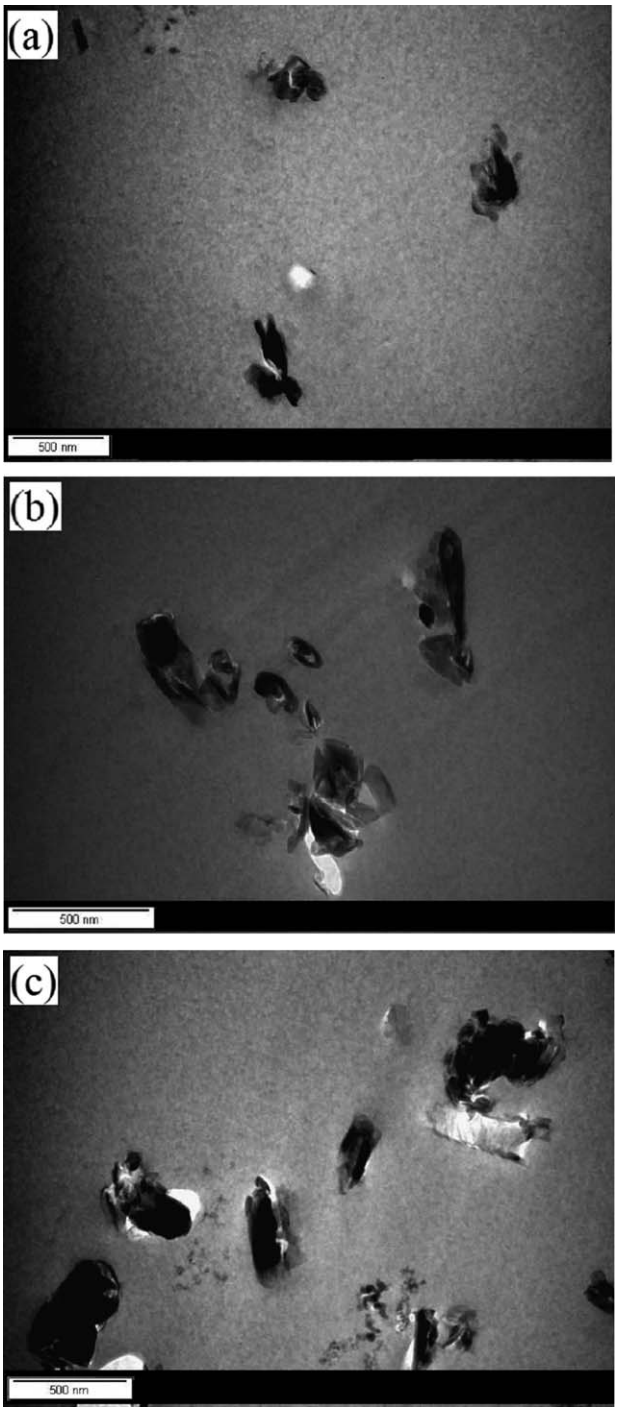

Figure 3. Dispersion of HNTs particles within cured VER (a) 1 wt % of HNTs, (b) 3 wt % of HNTs, and (c) 5 wt % of HNTs.

phase and a discontinuous phase. The continuous phase is the VER-rich regions in which a good dispersion of individual HNT clusters is clear. In contrast, the agglomeration of HNT clusters embedded in this continuous phase forms the rigid discontinuous phase.[13,16]

Toughness Properties

The results of fracture toughness and impact toughness are shown in Table IV. The results show that the addition of HNTs has led to enhanced toughness values for all VER/HNT composites samples. For example, compared to the fracture toughness of pure VER (1.81 MPa $m^{1/2}$), the fracture toughness of VER/HNT samples were higher with 17% increase for HNT loading of 1.0 wt %, 34% increase for 3.0 wt % loading, and 46% increase for 5.0 wt % loading. Similarly, the addition of HNTs at 1, 3, and 5 wt % increased the impact toughness of pure VER (1.52 kJ/m^2) by 93, 118, and 172%, respectively.

Figure 5(a) shows the fracture surface of pure VER which is flat and smooth except for some river line markings near the crack initiation site which indicates typical brittle fracture behavior or low fracture toughness.[43] In contrast, the non-planar fracture surfaces of VER/HNT nanocomposites are shown in Figure 5(b–d). These figures depict an increasing roughness of the fracture surfaces with increasing loading of HNTs. The roughness of the fracture surface is an indicator of the quantity of energy dissipated during fracture.[44] With increasing HNT content, the fracture surfaces of these samples become rougher and the crack bifurcation is more evident. Such visual features suggest crack path deflection due to the rigidness of HNTs in hindering crack propagation.[37,45]

SEM images in Figure 6(a–c) reveal micro-sized white fillers on the fracture surfaces of the VER/HNT nanocomposites. These fine white fillers are HNT clusters and are evenly distributed within the matrix. These clusters can increase toughness by stopping the propagation of cracks through interacting with passing cracks and resisting crack advancement.[13,46] Plastic deformation of VER around clusters is also evident. Plastic deformation and crack deflection by these clusters are the principal toughening mechanisms observed in this study.[16] These clusters are believed to resemble micro-sized rigid inorganic particles, which when confronting cracks hinder the crack propagation and cause crack deflection, twisting, and plastic deformation in particulate polymer composite.[47–49]

The effectiveness of HNTs in imparting toughness needs to be assessed against alternative fillers such as nanoclay or rubbery particles. In an attempt to improve the fracture toughness of vinyl-ester, nanoclay and/or core shell rubber (CSR) particles were used by Subramaniyan and Sun.[4] Their results showed that an improvement in fracture toughness of 12% was achieved by CSR, whereas the addition of nanoclay and nanoclay/CSR caused a reduction in fracture toughness by 16 and 6%, respectively. Therefore, HNTs may be preferable to nanoclay for improving the toughness of vinyl-esters.

Flexural Modulus and Strength Properties

The flexural modulus, flexural strength, and impact strength of VER/HNT composites are summarized in the Table V, and the improvements in these properties due to HNT addition is evident. With regards to flexural modulus, the addition of HNTs has led to an improvement from 2.90 GPa to 3.11, 3.31, and 3.42 GPa for HNT loading of 1, 3, and 5 wt %, respectively. The addition of HNTs caused a moderate increase in flexural strength and impact strength. When pure VER is reinforced with 1, 3, and 5 wt % HNTs, the flexural strength of resultant nanocomposites increased to 45.9, 51.1, and 56.5 MPa,

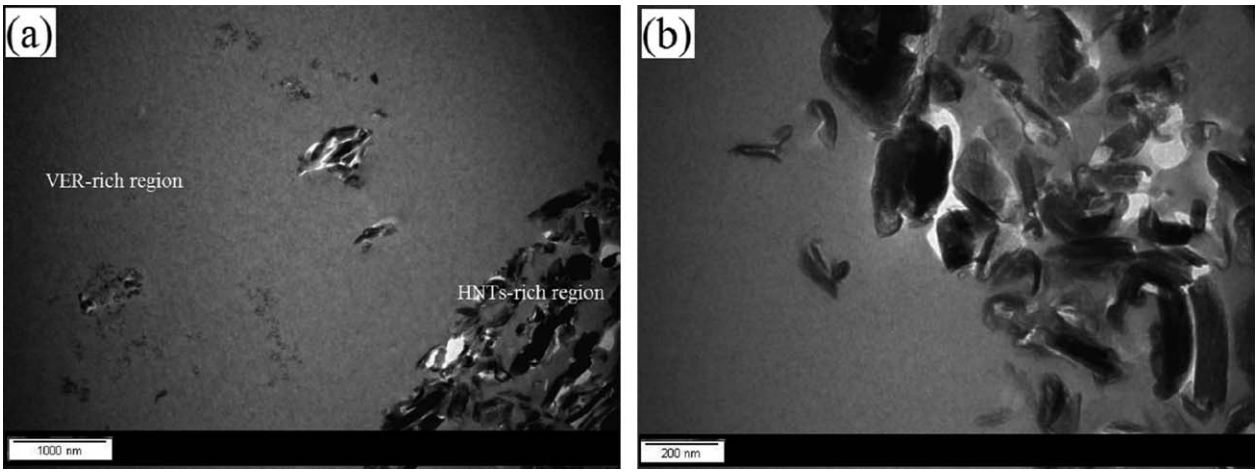

Figure 4. TEM micrographs of VER/HNTs Nanocomposites (a) VER-rich region and HNTs-rich region and (b) Spaces between HNTs particles cluster clearly filled by VER.

Table IV. Fracture Properties of VER and VER/HNTs Nanocomposites

Samples	HNT content (wt %)	Fracture toughness (MPa $m^{1/2}$)	Impact toughness (kJ/m^2)
VER	0	1.8 ± 0.1	1.5 ± 0.1
VER/1% HNTs	1	2.1 ± 0.2	2.9 ± 0.2
VER/3% HNTs	3	2.4 ± 0.1	3.3 ± 0.1
VER/5% HNTs	5	2.6 ± 0.1	4.1 ± 0.2

respectively. Similarly, the addition of HNTs at 1, 3, and 5 wt % increased the impact strength to 3.32, 4.12, and 4.45 kJ/m^2, respectively. Based on these results, the nanocomposites containing HNTs displayed increased modulus and strength properties when compared to neat VER. This observation is further supported by the fracture surface shown in Figure 7(a–d). When comparing Figure 7(a) of VER with Figure 7(b–d) of VER/HNT nanocomposites, the roughness and tortuousity of the fracture surfaces can be seen to increase with increasing HNT loading.

In general, the elastic modulus of a polymer matrix is enhanced by adding fillers that are rigid.[30,35] Since HNTs have higher elastic modulus (30 GPa) than VER (2.90 GPa) and by virtue of the rule-of-mixtures, an improved elastic modulus was obtained for all VER/HNT nanocomposites. On the other hand, with respect to strength of particulate reinforced polymer composites, the size (micro/nanoscale) of particles in relation to the specific

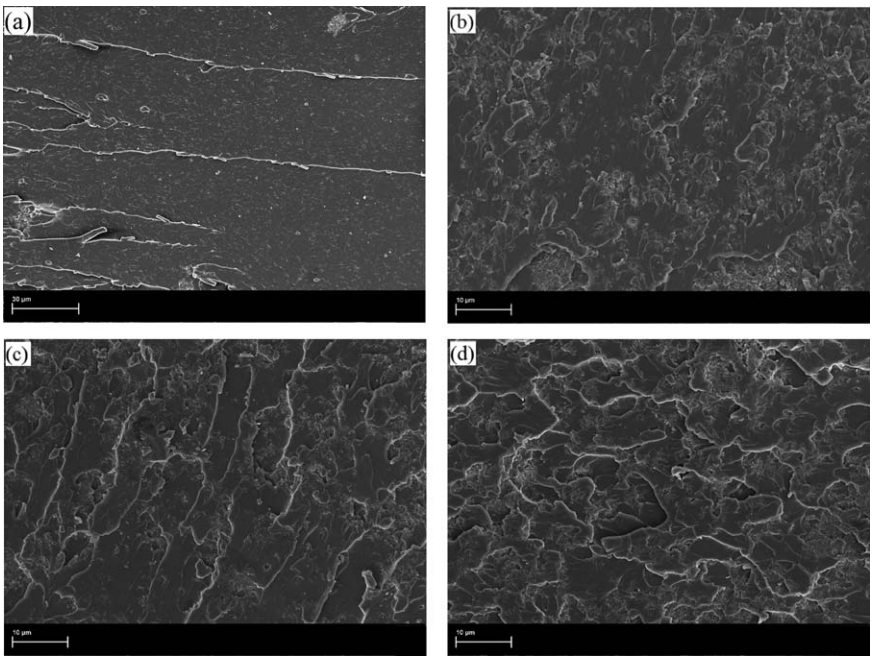

Figure 5. SEM images of fracture surfaces of (a) VER, (b) VER/HNTS composite with 1 wt % HNTs loading, (c) VER/HNTs composite with 3 wt % HNTs loading (d) VER/HNTs composite with 5 wt % HNTs loading. All samples had been subjected to fracture toughness test.

Applied Polymer SCIENCE

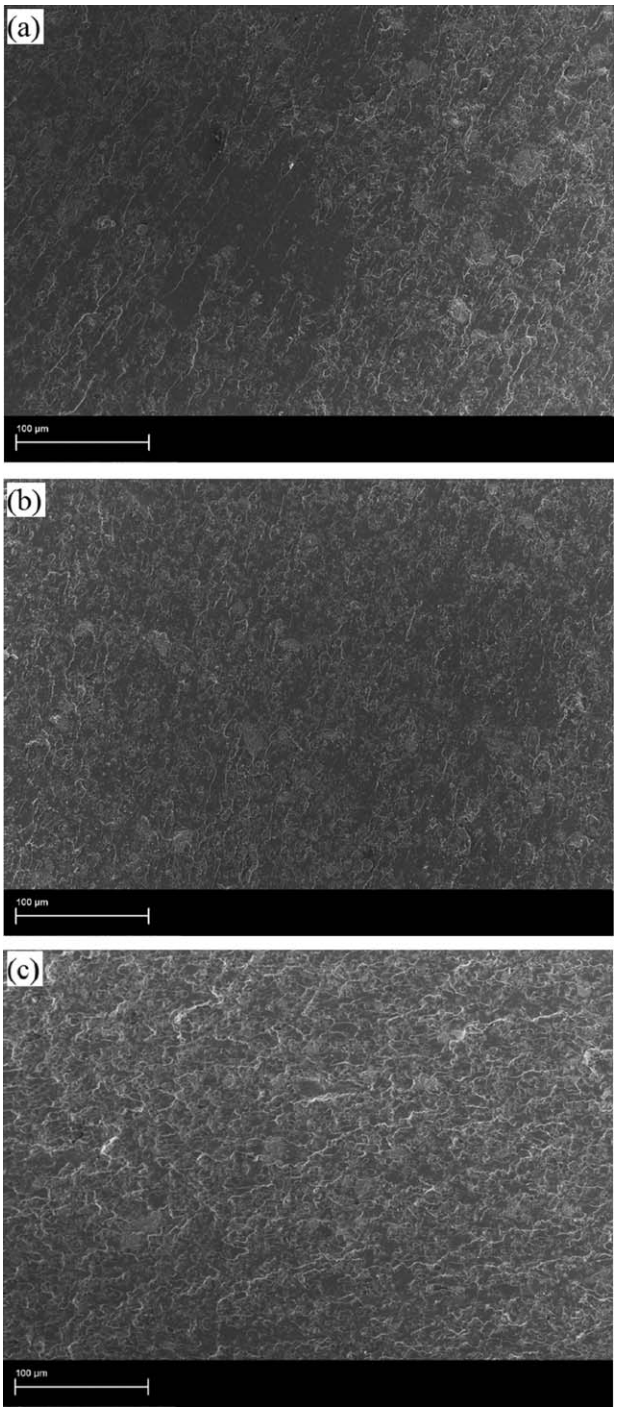

Figure 6. Fracture surfaces of VER/HNTs composites with (a) 1% wt of HNTs loading, (b) 3% wt HNTs loading, and 5% wt HNTs loading, showing crack deflection and plastic deformation around HNTs particle clusters.

surface area,[31] interfacial bonding between particles and matrix,[11] and degrees of particle dispersion,[50] are factors necessary for enhanced strength properties. These dynamics drive the load transfer between reinforcing particles and matrix which is efficient and ultimately results in better strength properties for the composites.[31,41]

Compared to micro-scales fillers the nano-scales fillers, such as the HNTs have a high specific surface area which allows dense interfacial interaction with the polymer matrix. Typically the specific surface area for halloysite nanotubes is about (65 m^2/g).[41] This large contact surface area can provide a favorable adhesion and bonding between filler and matrix which increases the strength of the composite. The SEM images in Figure 8 show this favorable adhesion between VER and HNTs, where there are no obvious cavities at the particle/matrix interfaces. Finally, the inter-tubular interaction between HNTs and VER can indicate a good bonding state between filler and matrix, which can serve to increase the strength properties.[41] All of these mechanisms mentioned above are believed to underpin the increased strength properties and overall mechanical properties of the nanocomposites of this study.

Comparisons with Theoretical Models

The experimental data on flexural modulus in this study were compared with well-known mathematical models of elastic modulus (Figure 9). One test of validity is the Reuss–Voigt model, which is an approximate theory, identifying upper and lower bounds of values for a predicted solution of elastic modulus for particulate reinforced composites. The validity of elastic modulus for most particulate micro- and nano-composites can be tested using the Reuss–Voigt model by comparing experimental data elastic modulus values with the lower and upper bounds provided by this model.[32] Results that fall between the bounds are believed to be valid. In the case of composites reinforced with a filler of large aspect ratio and strong adhesion between filler and matrix, the upper bound of Reuss–Voigt model is appropriate. In the case of rigid spherical fillers, the lower bound is applicable.[34,51] The model supports the validity of elastic modulus results in this study. All experimental and predicted data value fell between the upper bounds and lower bounds. Interestingly, the experimental data lie close to the upper bounds. This can be attributed to the large aspect ratio of HNTs and the good adhesion between HNTs and VER. Both the Paul model and the Guth model agree well with the experimental results. The assumption of a perfect adhesion between the particles and matrix underpins the Paul model.[30,31] Thus the experimental data is believed to support adequate adhesion between the filler and matrix in the nanocomposite samples. The microstructures observed by SEM and TEM also supported adequate interfacial bonding between HNTs and VER. The Guth model also assumes perfect adhesion between filler and matrix, but also assumes perfect dispersion, and large particle aspect ratio.[30,32] Thus the experimental results here support adequate adhesion between the filler and matrix, acceptable dispersion, and that the majority of HNTs were found to exist in a tubular shape with an aspect ratio of between 3 and 15.

Nonetheless, both models of Paul and Guth have over-predicted the modulus of the samples in this study for cases where the volume fraction increased to 5 wt %. This discrepancy is most likely explained by the formation of HNT clusters in the 5 wt % nanocomposites. These clusters within the samples can affect the load bearing capability and result in a lower elastic

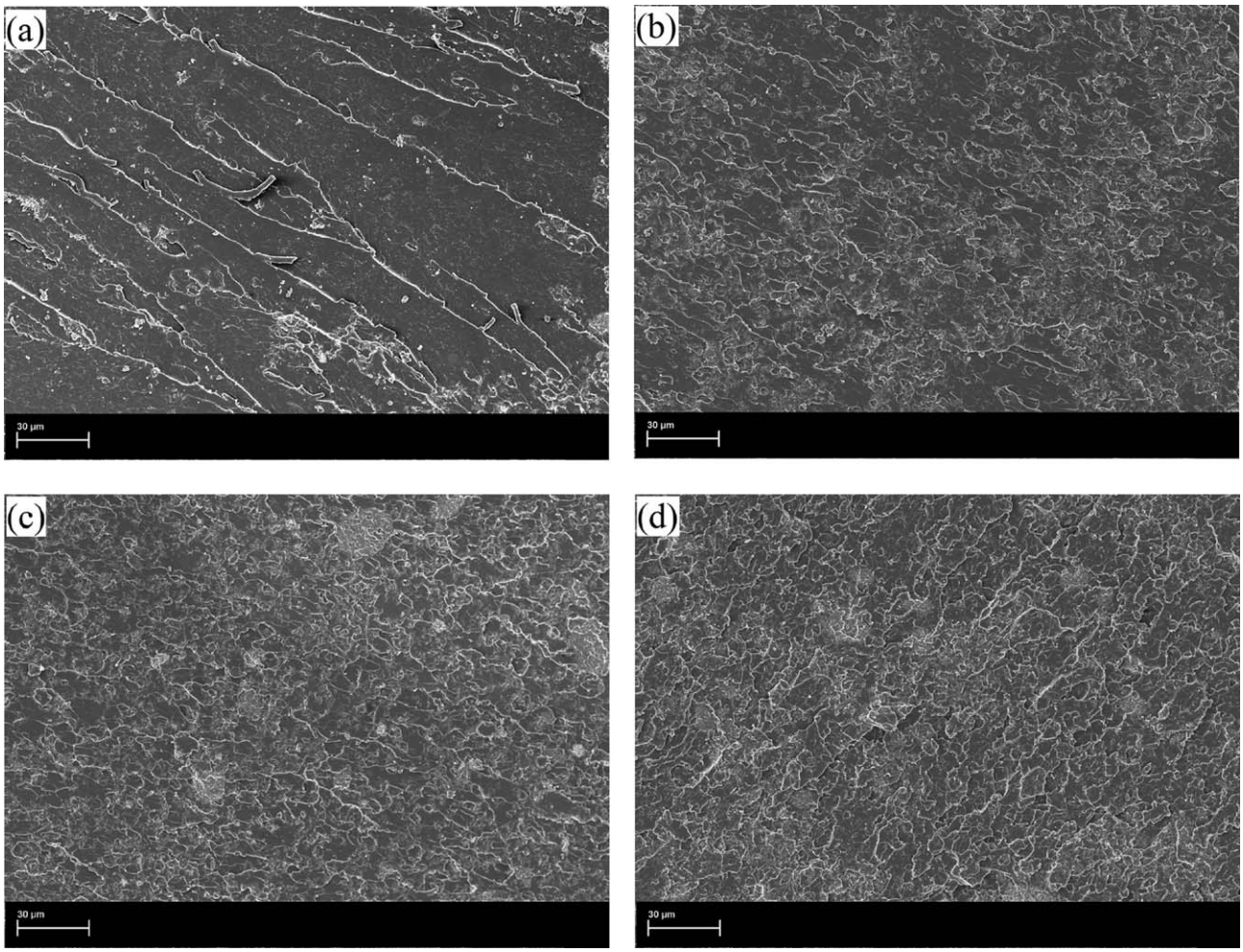

Figure 7. SEM micrographs of fracture surfaces of (a) pure VER/HNTS composite, VER/HNTs composites with 1 wt % HNTs loading, (c) VER/HNTs composite with 3 wt % HNTs loading, and (d) VER/HNTs composite with 5 wt % HNTs loading. All samples had been subjected to flexural strength test.

modulus.[33] At the same time, overall aspect ratio of HNTs can be reduced due to the formation of clusters[52] and also during processing due to the shearing effect which breaks the HNTs.[50] The models of Paul and Guth do not take into consideration the formation of clusters or the reduction in aspect ratio of the fillers. The Kerner model is a measure of validity for composite systems in which the modulus of filler is many times higher than the modulus of the matrix.[31,35] The relative modulus ratio of fillers to matrix in this study is low which explains the lack

Table V. Mechanical Properties of VER and VER/HNTs Nanocomposites

Samples	HNTs content (wt%)	Flexural modulus (GPa)	Flexural strength (MPa)	Impact strength (kJ/m^2)
VER	0	2.90 ± 0.04	42.0 ± 2.4	2.6 ± 0.1
VER/1% HNTs	1	3.11 ± 0.02	45.9 ± 2.1	3.3 ± 0.1
VER/3% HNTs	3	3.31 ± 0.05	51.1 ± 1.8	4.1 ± 0.1
VER/5% HNTs	5	3.46 ± 0.04	56.5 ± 2.0	4.5 ± 0.9

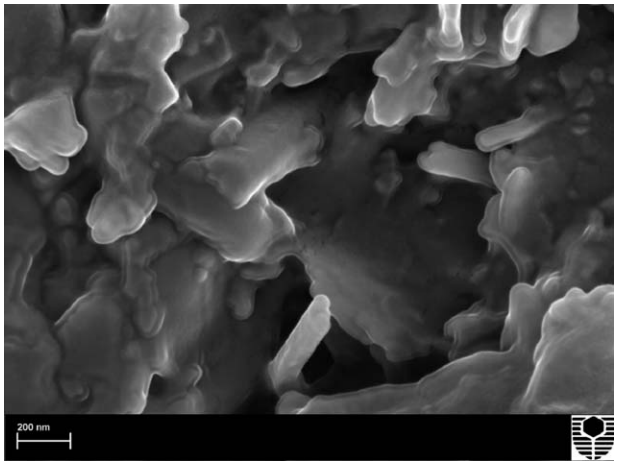

Figure 8. SEM micrograph showing favorable adhesion between VER and HNTs.

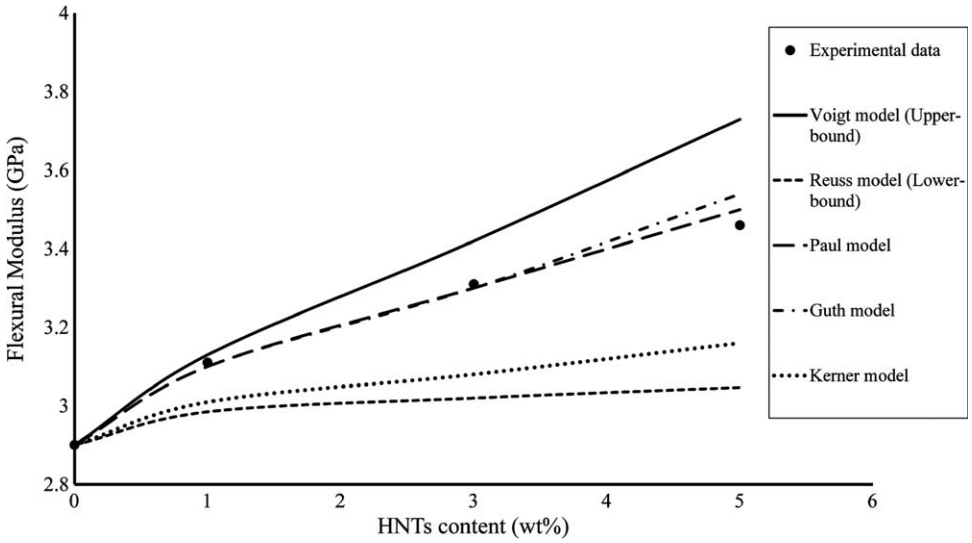

Figure 9. Comparison of experimental data for flexural modulus against HNTs content with results extrapolated from published models.

of agreement between experimental data when compared to the Kerner model. The study parameters applied to Frankle-Acrivos model (not shown) totally over-estimated the modulus of the samples in this study. The model uses the simple relative filler volume fraction (V_p/φ_{max}), thus only takes into consideration a partly dominant effect of particle packing efficiency on the elastic properties. The model neglects particle and matrix interfacial interactions, the Young's modulus and Poisson's ratio effects, which are all important factors that influence the elastic properties of composites.[31,33,34]

In summary, based on current findings and the results of other studies,[16,31,53,54] the aspect ratio of fillers, and, in particular, the state of adhesion between fillers and matrix are both significant factors that should be taken into account when predicting the elastic modulus of particulate-reinforced composites. The postulation that adhesion between fillers and matrix is a significant determinant of elastic modulus contradicts the findings of earlier studies as reviewed by Ahmed and Jones[30] and Fu et al.[32] In contrast to the results of this study, some of the earlier investigations suggested that adhesion between fillers and matrix was an insignificant or irrelevant factor in relation to the prediction of elastic modulus for particulate–polymer composites.

CONCLUSIONS

Pure VER and VER/HNT nanocomposites have been synthesized and characterized in terms of mechanical and fracture properties. HNTs were found to be an effective additive for improving the toughness of vinyl-esters. Enhancements in these properties were attributed to crack bridging, deflection, and plastic deformation in the vicinity of HNT clusters served to interact with cracks effectively to resist the advancement of the crack propagation. The enhancement in strength properties for VER/HNT composites was ascribed to the large aspect ratio of HNTs, good interfacial adhesion, good degree of dispersion, and adequate inter-tubular interaction. The good agreement of experimental data with models of Paul and Guth suggests that the aspect ratios of fillers, their dispersion within the matrix, and the state of interfacial adhesion are relevant to the prediction of elastic modulus for particulate reinforced polymer composites.

ACKNOWLEDGMENTS

We are grateful to our colleague Dr. Nobuo Tezuka for providing HNTs for this study. We would also like to thank Elaine Miller and Dr. Cat Kealley for their assistance with SEM imaging and XRD data collection.

REFERENCES

1. Yong, V.; Hahn, H. T. *Nanotechnology* **2004**, *15*, 1338.
2. Cauvin, L.; Kondo, D.; Brieu, M.; Bhatnagar, N. *Polym. Test.* **2010**, *29*, 245.
3. Shokuhfar, A.; Zare-Shahabadi, A.; Atai, A.-A.; Ebrahimi-Nejad, S.; Termeh, M. *Polym. Test.* **2012**, *31*, 345.
4. Subramaniyan, A. K.; Sun, C. T. *Compos. Part A: Appl. Sci. Manuf.* **2007**, *38*, 34.
5. Zeng, Q. H.; Yu, A. B.; Lu, G. Q.; Paul, D. R. *J. Nanosci. Nanotechnol.* **2005**, *5*, 1574.
6. Pavlidou, S.; Papaspyrides, C. D. *Prog. Polym. Sci.* **2008**, *33*, 1119.
7. Ismail, H.; Salleh, S. Z.; Ahmad, Z. *Int. J. Polym. Mater.* **2012**, *50*, 681.
8. Xie, Y.; Chang, P. R.; Wang, S.; Yu, J.; Ma, X. *Carbohydr. Polym.* **2011**, *83*, 186.
9. Lecouvet, B.; Gutierrez, J. G.; Sclavons, M.; Bailly, C. *Polym. Degrad.Stab.* **2011**, *96*, 226.
10. Rooj, S.; Das, A.; Thakur, V.; Mahaling, R. N.; Bhowmick, A. K.; Heinrich, G. *Mater. Design* **2010**, *31*, 2151.
11. Hedicke-Höchstötter, K.; Lim, G. T.; Altstädt, V. *Compos. Sci. Technol.* **2009**, *69*, 330.

12. Prashantha, K.; Schmitt, H.; Lacrampe, M. F.; Krawczak, P. *Compos. Sci. Technol.* **2011**, *71*, 1859.
13. Ye, Y.; Chen, H.; Wu, J.; Ye, L. *Polymer* **2007**, *48*, 6426.
14. Isik, I.; Yilmazer, U.; Bayram, G. *Polymer* **2003**, *44*, 6371.
15. Wetzel, B.; Haupert, F.; Friedrich, K.; Zhang, M. Q.; Rong, M. Z. *Polym. Eng. Sci.* **2002**, *42*, 1919.
16. Deng, S.; Zhang, J.; Ye, L.; Wu, J. *Polymer* **2008**, *49*, 5119.
17. Sultania, M.; Yadaw, S. B.; Rai, J. S. P.; Srivastava, D. *Mater. Sci. Eng. A* **2010**, *527*, 4560.
18. Marsh, G. *Reinforced Plast.* **2007**, *51*, 20.
19. Alhuthali, A.; Low, I. M.; Dong, C. *Compos. Part B: Eng.* **2012**, *43*, 2772.
20. Guo, Z.; Lei, K.; Li, Y.; Ng, H. W.; Prikhodko, S.; Hahn, H. T. *Compos. Sci. Technol.* **2008**, *68*, 1513.
21. Abdelwahab, M.; Agag, T.; Akelah, A.; Takeichi, T. *Polym. Eng. Sci.* **2012**, *52*, 125.
22. Ratna, D.; Khan, S.; Barman, S.; Chakraborty, B. *Open Macromol. J.* **2012**, *6*, 59.
23. Deng, S.; Zhang, J.; Ye, L. *Compos. Sci. Technol.* **2009**, *69*, 2497.
24. Lecouvet, B.; Sclavons, M.; Bourbigot, S.; Devaux, J.; Bailly, C. *Polymer* **2011**, *52*, 4284.
25. Marney, D. C. O.; Russell, L. J.; Wu, D. Y.; Nguyen, T.; Cramm, D.; Rigopoulos, N.; Wright, N.; Greaves, M. *Polym. Degrad. Stab.* **2008**, *93*, 1971.
26. Zhao, M.; Liu, P. *J. Thermal Anal. Calorim.* **2008**, *94*, 103.
27. Low, I. M.; McGrath, M.; Lawrence, D.; Schmidt, P.; Lane, J.; Latella, B. A.; Sim, K. S. *Compos. Part A: Appl. Sci. Manuf.* **2007**, *38*, 963.
28. Plati, E.; Williams, J. G. *Polym. Eng. Sci.* **1975**, *15*, 470.
29. Low, I. M.; Somers, J.; Kho, H. S.; Davies, I. J.; Latella, B. A. *Compos. Interfaces* **2009**, *16*, 659.
30. Ahmed, S.; Jones, F. R.; *J. Mater. Sci.* **1990**, *25*, 4933.
31. Dong, Y.; Chaudhary, D.; Ploumis, C.; Lau, K.-T. *Compos. Part A: Appl. Sci. Manuf.* **2011**, *42*, 1483.
32. Fu, S.-Y.; Feng, X.-Q.; Lauke, B.; Mai, Y.-W. *Compos. Part B: Eng.* **2008**, *39*, 933.
33. Yan, W.; Lin, R. J. T.; Bhattacharyya, D. *Compos. Sci. Technol.* **2006**, *66*, 2080.
34. Chan, C.-M.; Wu, J.; Li, J.-X.; Cheung, Y.-K. *Polymer* **2002**, *43*, 2981.
35. Kaully, T.; Siegmann, A.; Shacham, D. *Polym. Compos.* **2008**, *29*, 396.
36. Reynaud, E.; Jouen, T.; Gauthier, C.; Vigier, G.; Varlet, J. *Polymer* **2001**, *42*, 8759.
37. Stevanovic, D.; Kalyanasundaram, S.; Lowe, A.; Jar, P. Y. B. *Compos. Sci. Technol.* **2003**, *63*, 1949.
38. Guimarães, L.; Enyashin, A. N.; Seifert, G.; Duarte, H. l. A. *J. Phys. Chem. C* **2010**, *114*, 11358.
39. Handge, U. A.; Hedicke-Höchstötter, K.; Altstädt, V. *Polymer* **2010**, *51*, 2690.
40. Bigg, D. M. *Polym. Compos.* **1987**, *8*, 115.
41. Ismail, H.; Pasbakhsh, P.; Fauzi, M. N. A.; Abu Bakar, A. *Polym. Test.* **2008**, *27*, 841.
42. Joussein, E.; Petit, S.; Churchman, J.; Theng, B.; Righi, D.; Delvaux, B. *Clay Miner.* **2005**, *40*, 383.
43. Wang, K.; Chen, L.; Wu, J.; Toh, M. L.; He, C.; Yee, A. F. *Macromolecules* **2005**, *38*, 788.
44. Chen, B.; Evans, J. R. G. *Scripta Mater.* **2006**, *54*, 1581.
45. Tang, Y.; Deng, S.; Ye, L.; Yang, C.; Yuan, Q.; Zhang, J.; Zhao, C. *Compos. Part A: Appl. Sci. Manuf.* **2011**, *42*, 345.
46. Lee, J.-H.; Jung, D.; Hong, C.-E.; Rhee, K. Y.; Advani, S. G. *Compos. Sci. Technol.* **2005**, *65*, 1996.
47. Meng, J.; Hu, X. *Polymer* **2004**, *45*, 9011.
48. Wetzel, B.; Rosso, P.; Haupert, F.; Friedrich, K. *Eng. Fract. Mech.* **2006**, *73*, 2375.
49. Ye, Y.; Chen, H.; Wu, J.; Chan, C. M. *Compos. Sci. Technol.* **2011**, *71*, 717.
50. Ning, N.-y.; Yin, Q.-j.; Luo, F.; Zhang, Q.; Du, R.; Fu, Q. *Polymer* **2007**, *48*, 7374.
51. Alam, P. *Mech. Res. Commun.* **2010**, *37*, 389.
52. Gantenbein, D.; Schoelkopf, J.; Matthews, G. P.; Gane, P. A. C. *Appl. Clay Sci.* **2011**, *53*, 538.
53. Ahmad, F. N.; Jaafar, M.; Palaniandy, S.; Azizli, K. A. M. *Compos. Sci. Technol.* **2008**, *68*, 346.
54. Masouras, K.; Silikas, N.; Watts, D. C. *Dental Mater.* **2008**, *24*, 932.